Journal of the Brazilian Society of Mechanical Sciences and Engineering (2024) 46:6
https://doi.org/10.1007/s40430-023-04586-z

TECHNICAL PAPER

The improved inverse method for axial compressor based on quasi-three-dimensional model

Haijian Lou[1] · Hu Wu[1] · Chen Yang[2] · Qing Tang[1] · Jinguang Li[1]

Received: 26 September 2022 / Accepted: 7 November 2023 / Published online: 5 December 2023

Abstract
An improved and steady inverse method based on the time-marching solution of quasi-three-dimensional Navier–Stokes equations for axial compressors is proposed in this work. The main novelty of this paper lies in the derivation of a stable inverse design boundary condition based on the conservation of Riemann invariants in order to redesign the blade quickly, which is established on a reduced-order model. At the same time, in order to simulate the flow field of transonic axial compressors more accurately, the solver takes the blade radius and thickness into consideration in the direct mode. In addition, a detailed inverse design time step method is employed to guarantee the robustness. Two redesigned cases are presented, including a subsonic stream surface and a transonic stream surface. On this basis, a transonic fan is partially redesigned near the hub of the blade. Through the novel three-dimensional verification of ANSYS CFX, the result shows that the inverse method achieves higher efficiency and better effect in the partial redesign of axial compressors, which demonstrates the effectiveness of the new inverse method.

Keywords Axial compressor · Inverse method · S1 stream surface · Aerodynamic performance · Numerical simulation

1 Introduction

At present, the development of computational fluid dynamics provides a strong theoretical basis and technical support for the simulation of compressors [1, 2]. With the continuous progress of computer technology and numerical method, computational fluid dynamics has become more and more capable of capturing the compressor flow field. On this basis, the inverse method of axial compressors has also become a research hotspot. Many inherent advantages of inverse method greatly improve the efficiency of compressor redesign, save costs, and shorten the design cycle.

Technical Editor: William Wolf.

✉ Hu Wu
wuhu@nwpu.edu.cn

1 School of Power and Energy, Northwestern Polytechnical University, 127 West Youyi Road, Beilin District, Xi'an 710072, Shaanxi, People's Republic of China

2 Institute of Engineering Thermophysics, Chinese Academy of Sciences, 11 Beisihuanxi Road, Beijing 100190, People's Republic of China

Research on the inverse method of turbomachinery can be traced back to the 1940 s. Lighthill [3] first proposed the concept of the inverse method of blade profile. Based on dealing with the two dimensional incompressible potential flow equation, the numerical solution of the flow field was obtained with a prescriptive velocity distribution. After that, a method for obtaining the geometrical configuration by a given velocity distribution along the blade profile was put forward by Stanitz [4], who performed an inverse design on a turbine blade for the first time. In the late 20th century, Hawthorne [5, 6] made a success in an inverse design method on the blade profile with zero-thickness distribution. The inverse design was successfully extended to three dimensions by Dulikravich [7] afterward.

In 1990 s, Dang [8, 9] began to conduct in-depth research on the inverse design method, who creatively brought forward the permeable boundary conditions that are of great significance to the inverse method of turbomachinery. Starting from the inverse method of two dimensional plane cascades, and on the basis of continuous development, the governing equations range from two dimensional inviscid equations to three dimensional viscous equations. The permeable boundary condition assumes that during the process of blade geometry update, the blade wall has a slipping velocity, that is, the slipping boundary condition. The viscous stress on the wall is estimated using an empirical model-wall function. A new permeable boundary condition on the basis of the inverse method raised by Dang was advanced by Qiu [10] of Dang's research group; at the same time, so as to solve the influence of flow separation and tip clearance on the inverse method, a unified curved surface generation method for the blade was posed, which is based on the idea of least squares and NURBS curve. Hield [11] and Van Rooij [12–14], extended the inverse design method to multistages, which better solved the matching problem among multiple rows, making the inverse method more meaningful in engineering application. British scholar Zangeneh [15–17] based on Dang's permeable boundary conditions and the self-developed CFD solver, took the lead in adopting unstructured mesh, and combined optimization ideas with inverse method to establish a new set of inverse design system. A dual-point inverse design method was set up by Ramamurthy and Ghaly [18] from Canada, taking the load distribution near the stall point and near the peak efficiency point as the target load, which significantly improves the overall performance of the blade.

Yang [19, 20] from Dalian University of Technology made a lot of research in detail into the existence and uniqueness of the inverse method, and established a method to solve the non-unique problem. On this basis, Yang expanded the permeable boundary conditions and constructed an inverse design method system by solving the full three-dimensional Navier–Stokes equations based on the finite volume method. A loading-camber and static pressure-profile inverse design system was framed by Liu [21] from Northwestern Polytechnical University, who developed a series of more practical adminicular software, and carried out modification designs for a variety of axial compressors and achieved a good result.

In previous studies, it is shown that the loading-camber method has strong stability, while the pressure-profile method directly links the changes of the blade geometry with the flow parameters. Taking into account the advantages and disadvantages of loading-camber method and pressure-profile method synthetically, this paper combines inverse method on the basis of the accurate Riemann solution set up by Jin-Guang, Y [22] and the pressure-profile inverse method developed by Chen, Y [23] to advance a new loading-camber inverse method. The method based on the quasi-three-dimensional solver of axial compressors, adjusts the blade camber by the pressure change of the local blade profile, and finally obtains a new blade geometry. The advantage of this method is that it can quickly modify the location where the local flow structure is terrible, which greatly improves the redesign efficiency by comparison with fully three-dimensional cases. On the other hand, the method essentially belongs to loading-camber method, and the application results show that it is more stable. To the author's best knowledge, the new inverse method based on S1 steam surface of axial transonic compressor has not been implemented in open literature.

The remainder of this paper is organized as follows. Section 2 presented theoretical governing equations, specific numerical solution method, and detailed numerical verification. In Sect. 3, systematic inverse theory and execution process of the inverse method was revealed. Then, the effectiveness was validated in two application cases in Sect. 4. At the final, meaningful and innovative conclusions are summarized in Sect. 5.

2 Flow analysis method

It is presented that the transformation between S1 stream surface coordinate system and cylindrical coordinate system in Fig. 1.

$$(dm)^2 = (dz)^2 + (dr)^2 \tag{1}$$

Applying the basic assumption of the revolution surface to the RANS equations in the relative cylindrical coordinate system, the governing equations of any revolution surface (S1 stream surface) in the coordinate system(m, φ) can be obtained, where m represents the meridian coordinate and φ represents the relative angular coordinate.

The governing equation is followed as:

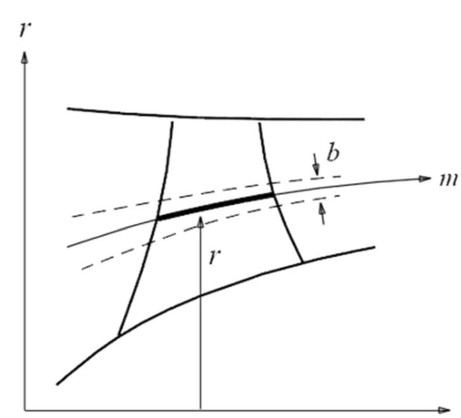

Fig. 1 Transform between S1 stream surface coordinate system and cylindrical coordinate system

$$\frac{\partial U}{\partial t}+\frac{1}{rh}\left[\frac{\partial rh(F-F_v)}{\partial m}+\frac{\partial h(G-G_v)}{\partial \varphi}\right]=S$$

$$U=\begin{pmatrix}\rho\\ \rho w_m\\ \rho w_\varphi\\ \rho E\end{pmatrix}, E_c=\begin{pmatrix}\rho w_m\\ \rho {w_m}^2+p\\ \rho w_m w_\varphi\\ \rho w_m H\end{pmatrix},$$

$$F_c=\begin{pmatrix}\rho w_\varphi\\ \rho w_\varphi w_m\\ \rho {w_\varphi}^2+p\\ \rho w_\varphi H\end{pmatrix}$$

$$E_v=\begin{pmatrix}0\\ \tau_{mm}\\ \tau_{m\varphi}\\ w_m\tau_{mm}+w_\varphi\tau_{m\varphi}+\frac{k\partial T}{\partial m}\end{pmatrix}, \tag{2}$$

$$F_v=\begin{pmatrix}0\\ \tau_{\varphi m}\\ \tau_{\varphi\varphi}\\ w_m\tau_{\varphi m}+w_\varphi\tau_{\varphi\varphi}+\frac{k\partial T}{r\partial\varphi}\end{pmatrix}$$

$$S=\begin{pmatrix}0\\ \frac{\rho(w_\varphi+\omega r)^2 r_m}{r}+p\left(\frac{r_m}{r}+\frac{h_m}{h}\right)-\frac{r_m}{r}\tau_{\varphi\varphi}-\frac{h_m}{h}\tau_{\eta\eta}\\ \frac{-\rho(w_\varphi+2\omega r)w_m r_m}{r}+p\left(\frac{h_\varphi}{rh}\right)+\frac{r_m}{r}\tau_{\varphi m}-\frac{h_\varphi}{rh}\tau_{\eta\eta}\\ \frac{\rho\omega^2 r^2 w_m r_m}{r}\end{pmatrix}$$

as usual, U is the conserved variable, and F, G is the convection flux, and F_v, G_v is the diffusion flux, and S is the source term taking the centrifugal force caused by changes in thickness(h) and radius(r) of the stream surface into consideration. Based on the cell-centered finite volume method, the JST scheme [24] coupled with a blended second-and fourth-order numerical dissipation is adopted to calculate the convective flux, while the diffusion flux is discreted by Gauss formula. The five-stage Runge–Kutta method can be used to deal with temporal discretization. In order to simulate the turbulence effect, a classic Baldwin–Lomax model [25] is applied. The implicit residual smoothing techniques and local-time stepping [26] are employed to accelerate the convergence of the solution process. The computational domains are discretized into structured H-type mesh. The boundaryconditions in the solver include non-reflective inlet, static-pressure outlet, periodic boundary, slip wall with wall function, and non-reflective mixing plane model. On this basis, a program to analyze the quasi-three-dimensional flow of axial compressors is developed.

In this paper, the pressure inlet boundary conditions are used. According to the characteristic analysis, the quasi-three-dimensional Navier Stokes Equation solving should be given three conditions at the subsonic inlet boundary. In this paper, the total temperature and total pressure of the incoming flow as well as the flow angle are given. In order to ensure that the propagation of characteristic waves in the flow field conforms to the characteristic direction, this paper extrapolates a one-dimensional Riemann invariant at the pressure inlet and constructs a non-reflective inlet boundary condition. The definition of the Riemann invariant is as follows:

$$R^-=\vec{v}_d.\vec{n}-\frac{2c_d}{\gamma-1} \tag{3}$$

The subscript 'd' indicates the parameters inside the flow field near the inlet. Riemann invariant can be used to solve for absolute velocity or sound velocity at the inlet. In practice, using it to calculate sound velocity can make the solution more stable, especially at low Mach numbers. Therefore, the sound velocity at the inlet can be expressed as:

$$c_b=\frac{-R^-(\gamma-1)}{(\gamma-1)\cos^2\theta+2}\left\{1+\cos\theta\sqrt{\frac{\left[(\gamma-1)\cos^2\theta+2\right]c_0^2}{(\gamma-1)(R^-)^2}-\frac{\gamma-1}{2}}\right\} \tag{4}$$

In the equation, θ is the angle of the airflow relative to the inlet, c_0 is the stagnation sound velocity, and is calculated by the following equations, respectively.

$$\cos\theta=-\frac{\vec{v}_d\cdot\vec{n}}{\|\vec{v}_d\|_2} \tag{5}$$

$$c_0^2=c_d^2+\frac{\gamma-1}{2}\|\vec{v}_d\|_2^2 \tag{6}$$

In the equation, $\|\vec{v}_d\|_2$ is the total velocity of the internal boundary, and the normal vector $\vec{n}$ points to the outside of the computational domain. Other physical quantities such as static pressure, static temperature, density, and velocity can be determined by the following equation.

$$T_b=T_0\left(\frac{c_b^2}{c_0^2}\right), p_b=p_0\left(\frac{T_b}{T_0}\right)^{\frac{\gamma}{\gamma-1}}, \quad \rho_b=\frac{p_b}{RT_b}, \|\vec{v}_b\|_2=\sqrt{2c_p(T_0-T_b)} \tag{7}$$

2.1 Numerical verification in analysis module

For the purpose of verifying the accuracy of the flow solver in simulating the quasi-three-dimensional flow of the transonic compressors, a medium-load transonic fan-NASA Rotor 67 [27] is selected as the research object, and any rotating surface is intercepted in the coordinate system to generate the computational grid. The numerical simulation results of this type of axial compressor are compared with the experimentally measured contour results in below.

The comparison of the relative Mach number distribution calculated by present codes and reported in the NASA paper near the peak efficiency operating point at three distinct sections along the blade span is presented from Fig. 2 to Fig. 4. As shown in the figures, the calculation results are in good agreement with the experimental values, and numerical calculations can more accurately simulate the flow details in the actual flow field. The calculation results correctly

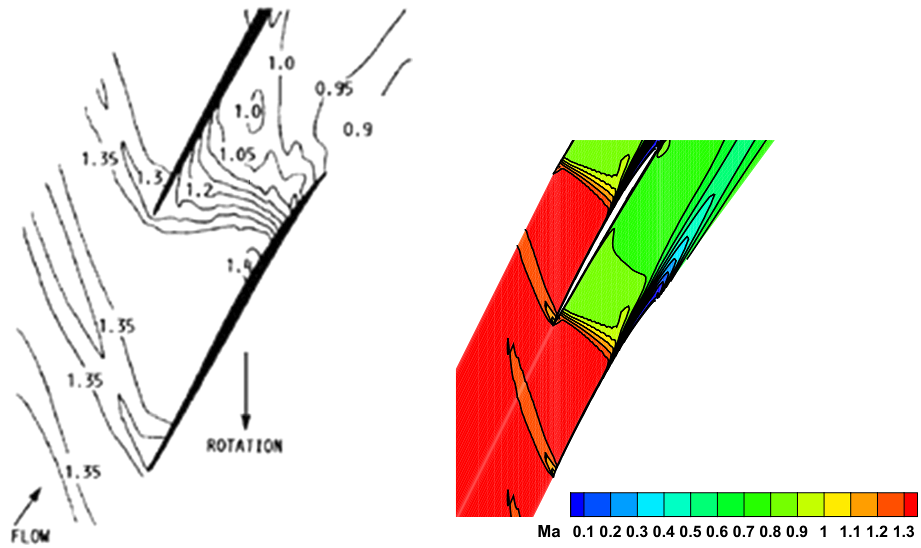

Fig. 2 The flow comparison between experiment(left) and simulation(right) at 90% span of Rotor 67

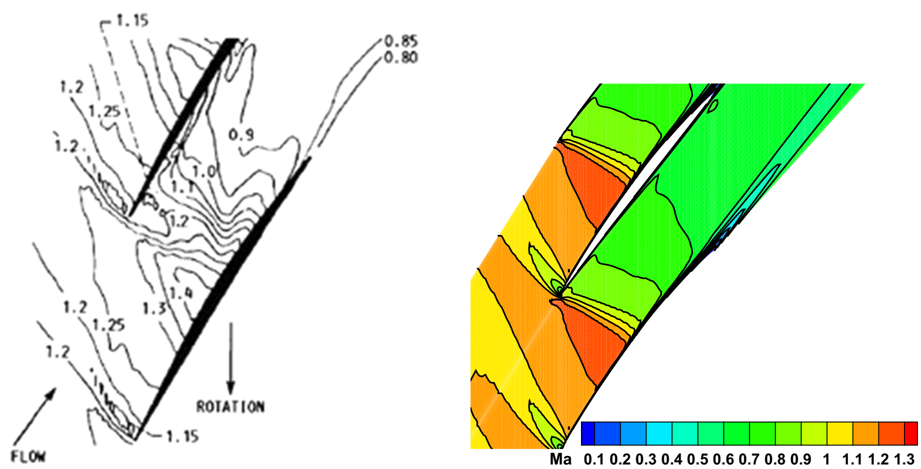

Fig. 3 The flow comparison between experiment(left) and simulation(right) at 70% span of Rotor 67

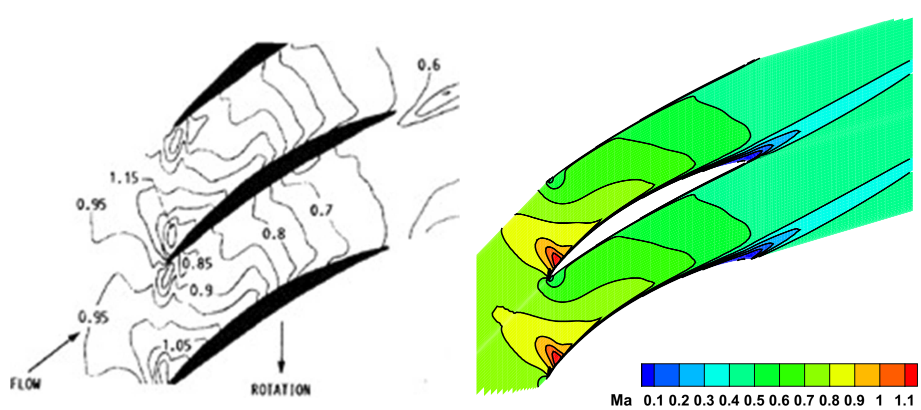

Fig. 4 The flow comparison between experiment(left) and simulation(right) at 30% span of Rotor 67

capture the shock wave structure of the flow field and have a higher resolution.

The cells used in the numerical simulation is 160*60. The convergence requirement of the Numerical method in this paper is that the calculated residual is reduced to −6. From Fig 2 it can be seen that at 90% span of the blade, due to the higher blade rim speed, the relative Mach number of the blade channel inlet has reached about 1.35, and the calculation is consistent with the experimental result. In addition, the experimental flow field has an oblique shock wave attached to the leading edge of the blade and a normal shock wave in the channel. The shock wave in the channel does not completely intersect the shock wave at the leading edge. The calculated position of the normal shock wave in the blade channel is also in good agreement with the experimental value.

In Fig 3, at 70% span of the blade, the relative Mach number of the inlet is about 1.25, and a normal shock wave appears in the blade channel. It can be seen from Fig. 4 that there is no obvious shock wave in the blade channel at 30% span of the blade. The relative Mach number of the inlet is about 0.95, and most areas of the flow field at subsonic velocity, but there is a local supersonic zone near the leading edge of the suction surface. By comparison, it can be seen that the numerical solution can correctly simulate the flow details in the blade channel, and the numerical method adopted in this paper has a high accuracy in capturing shock waves and can meet the engineering accuracy requirements.

3 The improved inverse method

When designing a compressor, the aerodynamic performance parameters of the compressor are the design goals of the designers. In traditional methods, designers continuously modify the geometric parameters of the blades to optimize the aerodynamic performance of the compressor. In the inverse design process, designers directly control the aerodynamic parameter distribution on the blade surface, making the control of the internal flow of the compressor more intuitive and closely related to the aerodynamic performance of the compressor.

The use of CFD method for solving the internal flow field of a compressor has higher accuracy and does not require empirical assumptions. Following the development of inverse problem design methods, it is necessary to establish the correlation between the internal flow field of a compressor and blade geometry based on CFD solution.

Based on the theory of the S1 stream surface viscous flow solver and the inverse method theory, this paper develops a quasi-three-dimensional inverse method that is distinct from the full three-dimensional, and takes the different sections of the blade as the design object of the inverse calculation. Compared with the full three-dimensional viscous inverse design, the quasi-three-dimensional inverse design has unique advantages. It can modify the design where there are locally undesirable flow details, and does not need to redesign the entire field, which greatly improves the inverse resigned efficiency. Based on relevant domestic research, this paper combines the advantages of two inverse design methods and creates a new and improved design method.

The inverse method of loading camber is to solve the geometry of the blade camber by giving the distribution of load on the blade surface. Dang from Syracuse University in the United States first proposed the inverse design method of updating the curved surface of the blade using a given blade surface load distribution. This method was initially established on the basis of solving two-dimensional inviscid Euler equations, and later continuously improved and developed, gradually applied to the full three-dimensional viscous solution.

Dang’s early research on inverse method was based on solving the inviscid Euler equation, so a permeable boundary condition was adopted at the wall, which means that the velocity direction of the airflow near the wall is tangent to the wall. Adjust the direction of wall velocity based on the given pressure load, while completing the update of the curved surface in the blade.

The advantage of this method is that the blade load reflects the work transfer between the blades and the airflow. By adjusting the load, the amount of work added to the airflow by the compressor blades can be effectively controlled, thereby controlling the total pressure ratio of the rotor blade outlet and the airflow angle of the stator blade outlet and other parameters. The concrete expression follows:

$$(V_y{}^{\pm})_{new}=V_{y,avg} \pm \frac{1}{2}(\Delta V_x f_x + V_{x,avg}T_x) \tag{8}$$

$$(p^{\pm})_{new} = p_{avg} \pm \frac{1}{2}\Delta p \tag{9}$$

$$f(x) = \int_0^x \left(\frac{V_{y,avg}}{V_{x,avg}} - \frac{1}{4}\frac{\Delta V_x}{V_{x,avg}}T_x\right)dx \tag{10}$$

where $V_{x,avg}$,$V_{y,avg}$,p_{avg} respectively represent the average value of the axial and circumferential velocity and pressure before the update, and Δp,ΔV_x indicate the pressure load and the difference between axial velocity of the two surfaces. $V_{y,new}$, and p_{new} represent the updated circumferential velocity and static pressure. f_x, and T_x respectively represent axial variation rate of mid-camber and blade thickness.

Despite continuous improvement of the permeable boundary conditions, this method still faces two issues: firstly, the implementation procedure of the loading-camber inverse method has no direct relationship with the actual aerodynamic parameters. Secondly, the phenomenon of airflow separation has a significant impact on the method. Due to the complex internal flow field of an axial-flow compressor, the existence of tip clearance vortices and corner vortices is inevitable. When there is a phenomenon of flow separation in the calculation, the tangential condition between the flow inside the separation area and the wall cannot be met, which directly affects the geometric update of the blade and even leads to divergence in the calculation.

In order to effectively control the flow structure on the blade surface more directly, designers have developed an inverse problem design method that directly controls the static pressure distribution on the blade surface. To ensure the stability and accuracy of inverse calculations, Liu established a new pressure-profile method. In order to ensure the conservation of flow characteristic variables at the wall before and after updating the blade profile, Liu constructed a new inverse design boundary condition using the conservation of Riemann invariants.

The blade suction and pressure surface static pressure distribution is taken as the design variables while the blade suction and pressure surface profile is the design goal. The surface profile will continue to change until the prescriptive static pressure distribution is satisfied during the design calculation course. The new method is more flexible, and the main advantage is that it can achieve more refined control of the flow field near the blade surface and in the blade channel, so as to achieve design goals such as reducing separation and changing the intensity and position of the shock wave. The concrete expression follows:

$$R^{\pm} = v_n^{\pm} \mp \frac{2c^{\pm}}{\gamma - 1} \tag{11}$$

$$\left(v_n^-\right)^{new} = \frac{2}{\gamma - 1}\sqrt{\frac{\gamma}{\rho^-}}\left(\sqrt{p^-} - \sqrt{\left(p^-\right)^{new}}\right) \tag{12}$$

$$\left(v_n^+\right)^{new} = \frac{2}{\gamma - 1}\sqrt{\frac{\gamma}{\rho^+}}\left(\sqrt{\left(p^+\right)^{new}} - \sqrt{p^+}\right) \tag{13}$$

$$\Delta s = \Delta t \cdot v_n \tag{14}$$

It can be seen from the Eqs. 12, 13 that the virtual normal velocity of the wall is driven by the static pressure difference before and after the update.

The pressure-profile method also has certain disadvantages in the actual implementation process. Because its essence is to directly modify the geometry of the blade surface, the pressure adjustment margin of this method is narrow, otherwise the calculation is difficult to converge.

Taking the limitations of the above two methods into consideration, on the basis of which, this article develops an improved inverse method. The concrete expression follows:

$$\Delta f = \frac{1}{2}\left(\left(v_n^-\right)^{new} n_\theta^- + \left(v_n^+\right)^{new} n_\theta^+\right)\Delta t \tag{15}$$

$$\Delta t = \min\left(\frac{0.01c}{\max\left(v_i\right)}, \Delta t_{flow}, 0.02\right) \tag{16}$$

Equation 15 presents that by averaging the virtual velocities of the suction and pressure surfaces to obtain the displacement of the camber, while an optimal time step is given in Eq. 16, in order to converge at the fastest rate during the inverse calculation.

3.1 Execution process of the inverse method

As similar as the course of typical inverse method, the new method established in this paper mainly includes the following steps: read the calculation grid, input files, boundary conditions, and target pressure load; calculate the flow field through the flow solver and compare it with the target load, then calculate the virtual displacement of the camber; superimpose the thickness of the blade on the basis of the new camber, update the calculation grid, and continue to solve the flow field until the whole process converges. The execution procedure is presented in Fig. 5.

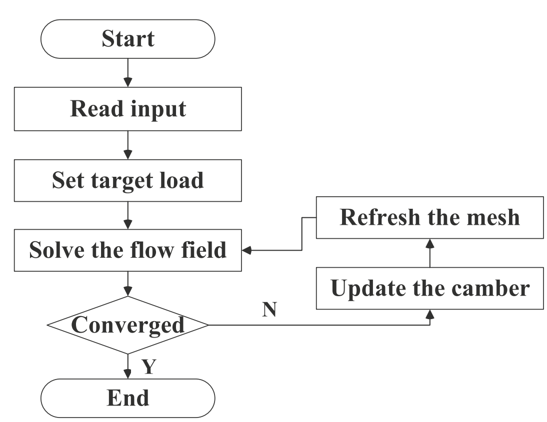

Fig. 5 The execution procedure of the inverse method

4 Results and analysis

4.1 Blade recovery test

In order to validate the effectiveness of the developed inverse design method, it is necessary to conduct a blade-recovery test. The test demands to compare the blade geometry calculated by the inverse method with the target geometry to ensure the accuracy of the inverse method. At the same time, it is also necessary to compare whether the flow field of the final calculation in the analytical and inverse mode is consistent to ensure the compatibility of the inverse method.

Figure 6 shows the convergence history of the inverse calculation at the recovery test of a typical transonic compressor cascade. The convergence requirement of the inverse method in this paper is that the calculated residual is reduced to −5, and the target load is basically the same as the blade load calculated. As it is visible from the convergence curve of the recovery test, the inverse calculation process is more oscillating than the residual in the analytical mode, which is mainly because the inverse calculation process is updated to a new geometry every 10 steps. The whole calculation takes 3 min to converge on the CPU-i5 4690K, which presents the high calculation efficiency.

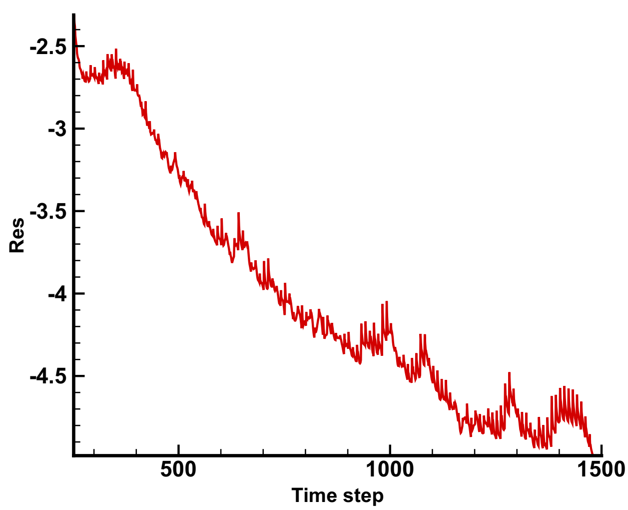

Fig. 6 The convergence history of the recovery test

The comparison diagram of the initial blade shape, the target blade shape, and the blade shape calculated is given below, as shown in Fig. 7. In the figure, the dotted line, solid line, circled line represent the initial blade, the blade obtained by the inverse calculation, and the target blade, respectively. The solution in the above figure refers to that the blade recovery test is very successful, and the final calculated convergent blade shape is basically the same as the target blade shape. On the other hand, obviously, apart from the less deviation near the trailing edge of the blade, the other parts of the load are in good agreement as it is visible in Fig. 7.

Figure 8 shows the relative Mach number diagrams obtained in the direct and inverse mode. From the cloud diagram, the recovery result of the inverse method is basically consistent with the convergence result of the direct calculation.

From an overall point of view, the recovery test basically achieves the design goal. Through this example, it is verified that the inverse design method developed in this paper has a certain accuracy and precision.

4.2 Application of the improved method in an axial fan

This section selects the typical S1 flow surface as the research object and carries out a modification design on it, so as to apply the quasi-three-dimensional inverse design method developed in this paper in engineering areas. By the

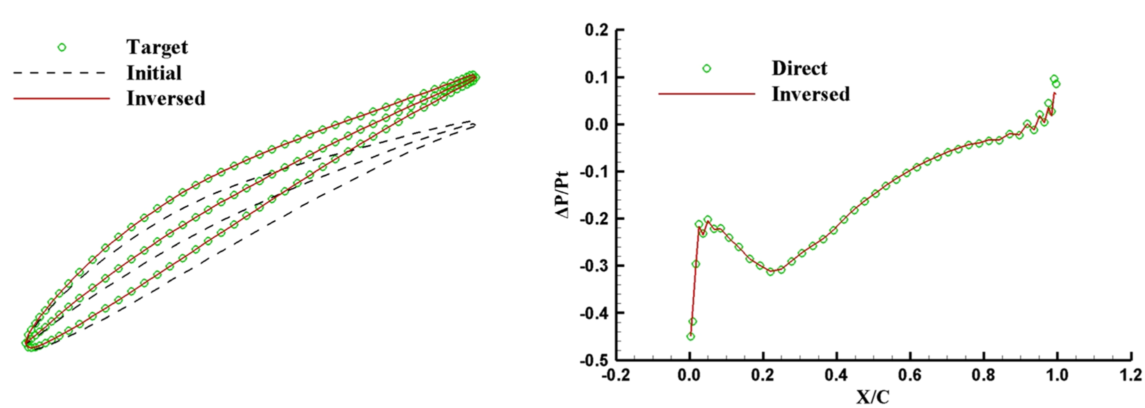

Fig. 7 The comparison of blade shapes and load [28] before and after the test

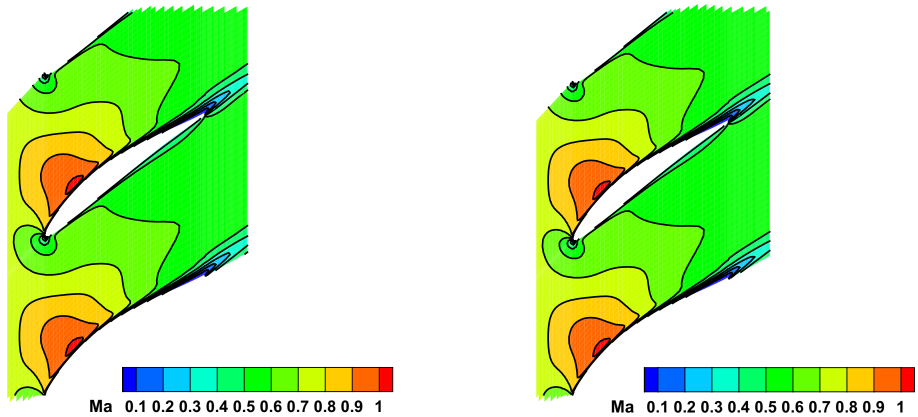

Fig. 8 The comparison of flow field before(left) and after(right) the test

readjustment of the blade surface load distribution, the effect of improving its aerodynamic performance is achieved.

When verifying the flow solver, a numerical simulation was carried out on the mid-load transonic fan NASA Rotor 67. From the simulation results, the flow field at different distinct sections along the blade span has shown different flow characteristics. Between the hub and 30% span, except for the local supersonic zone, the rest are flowing at subsonic velocity without obvious shock waves. From the 50% span to the tip, a strong shock wave appears in the flow field. The closer to the tip, the stronger the shock wave intensity. It is found from Figs. 2, 3, 4 that the boundary layer near the trailing edge of the blade hub is separated, resulting in a large flow loss and a decrease in aerodynamic performance. The shock wave from the middle to the tip of the blade will also cause a certain shock wave loss. In this section, these two different flow sections are designed and modified based on the compressor load distribution strategy.

4.2.1 Modification to suppress separation of the subsonic cascade

Based on the analysis of the flow mechanism of the subsonic cascade, this section makes a reasonable distribution of the blade surface load distribution to suppress the flow separation of the trailing edge. The front-loaded method should be adopted for the subsonic blade type on basis of the compressor load distribution strategy theory. The diffusion procedure of the front-loaded airfoil is mainly completed in the first half, and the diffusion is slow in the second half, which has the widest working range and the best aerodynamic performance. In this paper, the blade surface load is adjusted as follows: (1) the load at the leading and trailing edge is set to 0; (2) the front-loaded method is adopted, with the leading edge to 30 percent of chord, the load increases rapidly from 0 to the maximum value, and then slowly reduces to 0, as visible in Fig. 9.

From the comparison between Fig. 9, obvious changes have taken place after the blade modification. It is caused by the front loading; the blade surface load after the

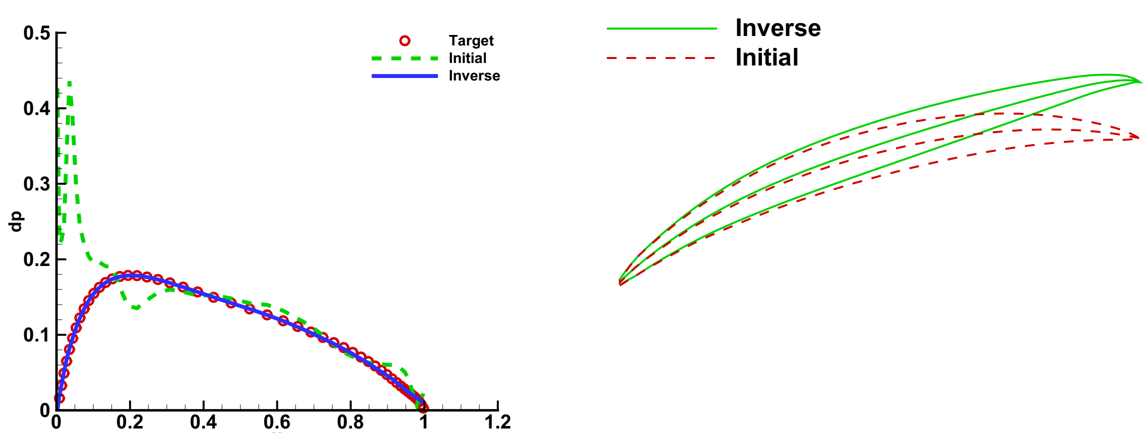

Fig. 9 The load distribution [27] and blade shapes before and after the modification

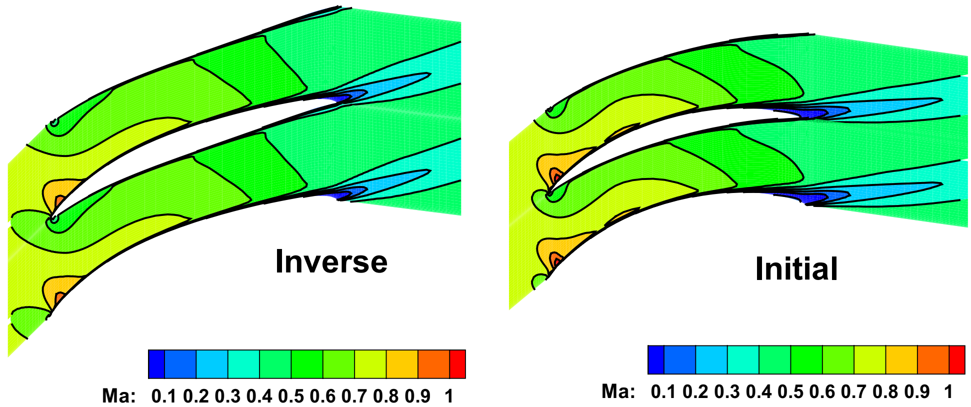

Fig. 10 The comparison of flow field before and after the redesign

inverse calculation converges is basically the same as the target load, which is in line with the front loading method. The solution in Fig. 10 refer to the fact that the relative Mach number near the trailing edge is larger than that of the original blade after the blade is modified, the reason for which is that most of the load is concentrated in the front half; the air flow in the second half slows down steadily, which reduces the separation of the trailing edge, therefore aerodynamic performance is improved by reducing flow loss.

In summary, the application of the front loading method to adjust the blade surface load distribution can well suppress the flow separation at the trailing edge of the subsonic blade profile, reduce the flow loss, and achieve the purpose of improving its aerodynamic performance.

4.2.2 Modification design of the transonic cascade

Compared with the subsonic cascade, the transonic cascade has a higher load, and its loss is mainly composed of the blade loss caused by the shock wave and the shock wave loss. Reasonable adjustment of shock wave position and control of shock wave intensity is an effective means for transonic blade modification. In this part, the section at 50% span is taken as the research object, and the design is modified to improve the aerodynamic performance of the blade.

As visible in Fig. 3, a thicker boundary layer is produced after the shock wave in the blade channel, which causes a certain flow loss. Therefore, the purpose of the modification in this part is to adjust the load distribution in order to reduce the flow loss caused by the shock wave.

Based on the load distribution strategy for the supersonic cascade and the principle of ensuring that the total load integral value remains unchanged, the blade surface load in this section is adjusted as follows: (1) the load at the leading and trailing edge is 0; (2) when adjusting the maximum load, the position of the maximum load value remains unchanged to ensure that the shock wave position remains unchanged; (3) ensure that the load is smooth in the first half to reduce the wavefront Mach number, and the load in the second half changes slowly to prevent shock-boundary layer interference from causing relatively high

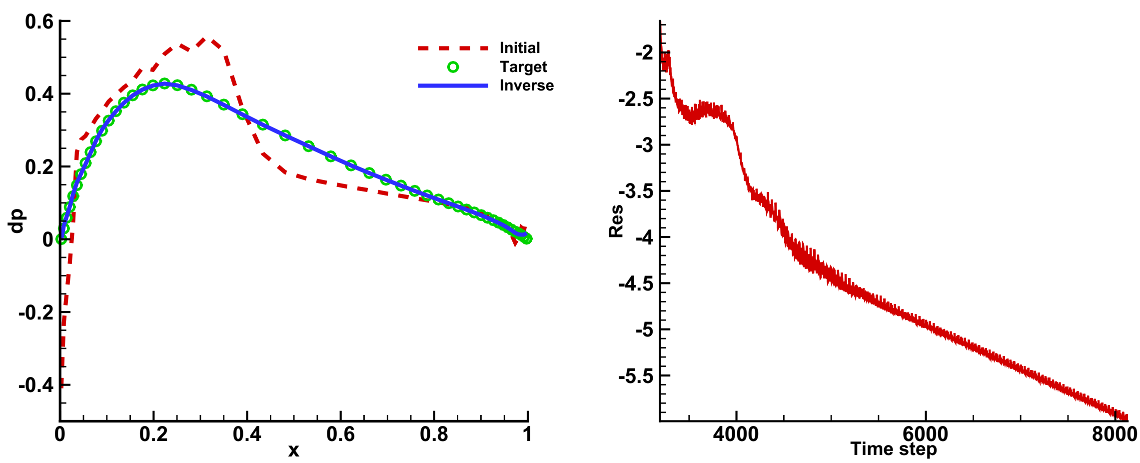

Fig. 11 The load distribution [27] of original blade and redesigned blade, and the convergence history

flow losses. The final adjusted load distribution is shown in Fig. 11.

The calculation results after the modification are given below. First, the calculation convergence curve is given, as visible in Fig. 11. After the analysis mode, the calculation is roughly advanced by 6000 steps when the residual drops to -5 and the inverse calculation converges. The surface load of the blade after the modification converges in Fig. 11 to basically the same as the target load, which satisfies the convergence condition.

From the blade shape comparison diagram in Fig. 12, the result reveals that the blade shape after the design modification has little change compared with the original. Next, the characteristics of the flow field in the direct and inverse mode is analyzed by comparing the relative Mach number diagram shown in Fig. 13. The result refers to that the intensity of the shock wave after the modification becomes weaker, but the position of the shock wave is basically unchanged, and the boundary layer behind the shock wave is obviously thinner to achieve the purpose of modification.

It can be concluded from the above that the modified design of the transonic blade reduces the loss caused by the shock wave and suppresses the shock wave-boundary layer interference, which improves the aerodynamic performance of the blade.

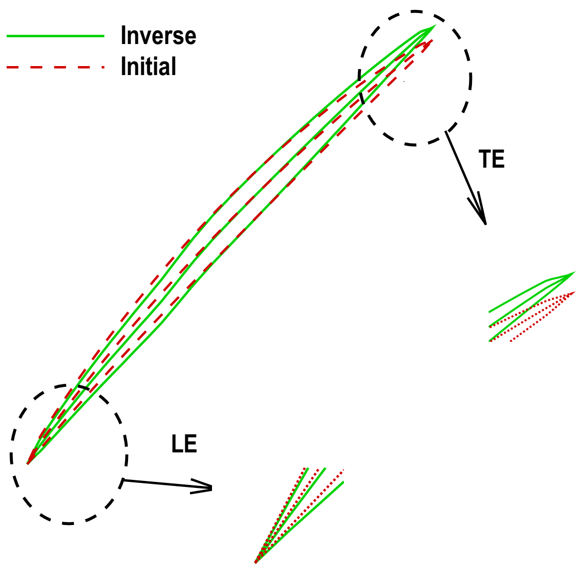

Fig. 12 The change of blade profile before and after the redesign

4.2.3 Modification and verification of Rotor 67

In the previous section, the flow field of the Rotor 67 transonic fan with 10% span and 50% span has been analyzed, and the blade profile has been modified and redesigned by reasonably adjusting the blade surface load distribution. In order to verify whether the aerodynamic performance of the entire blade is improved by the modified design mentioned above, this paper reconfigures the partial section of the original three-dimensional blade to obtain a new three-dimensional blade. Considering that the flow loss near the hub of Rotor 67 is particularly serious, this section will modify the 10% span. In order to make the blade smooth, 0 to 30% span is used for a smooth transition of the blade shape, and 50% to 90% span remains unchanged, and the commercial software ANSY-CFX is applied to perform full three-dimensional verification of the obtained new blade.

Figure 14 shows the flow field at 10% span of the blade before and after the modification. The section is designed in a front loading mode, which reduces the flow separation near the trailing edge by reducing the bending angle of the blade. The relative Mach number at 20%, 50%, 90% span are revealed in Fig. 15, 16, 17, respectively.

The solution in Figs. 14, 15, 16, 17 refers to that, on the one hand, after the modified design of the 10% span section, the boundary layer near the hub becomes thinner, the flow separation is reduced, and its aerodynamic performance is improved; on the other hand, the wake of the blade below

Fig. 13 The comparison of flow field before and after the redesign

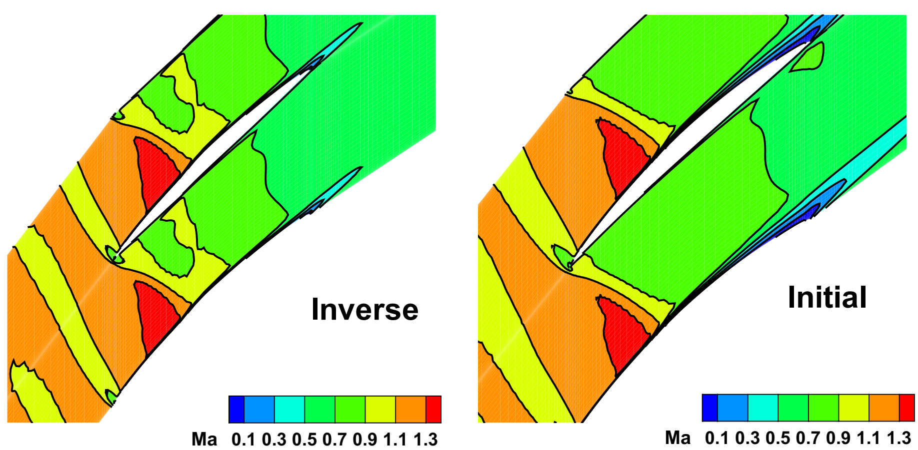

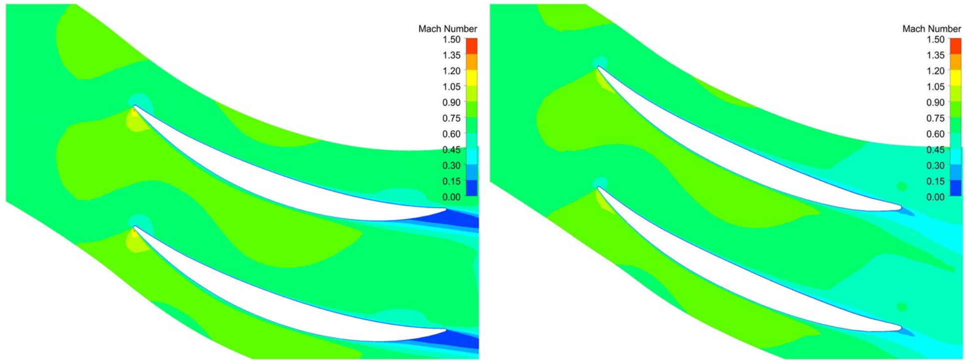

Fig. 14 The flow at 10% span of Rotor 67 between the original(left) and new(right) blade

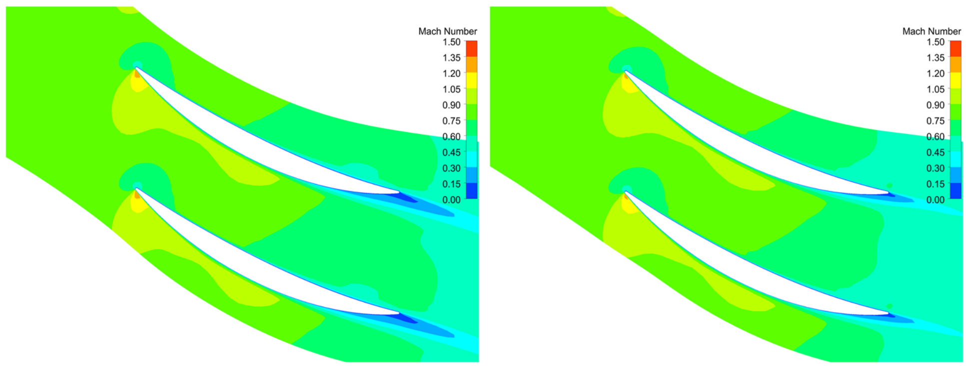

Fig. 15 The flow at 20% span of Rotor 67 between the original(left) and new(right) blade

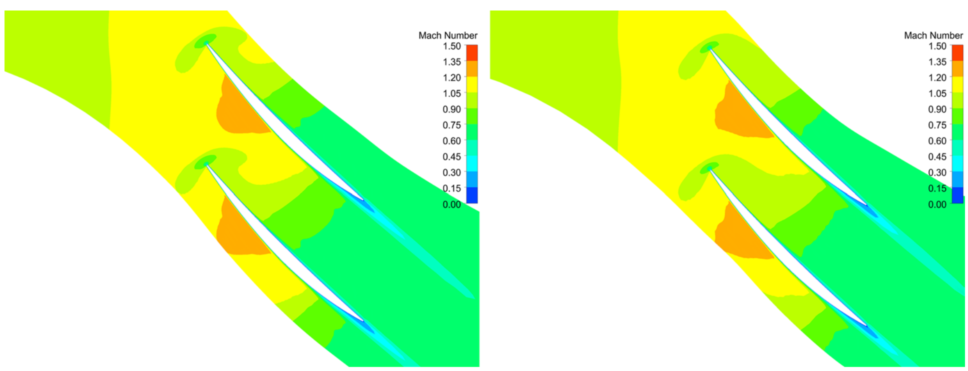

Fig. 16 The flow at 50% span of Rotor 67 between the original(left) and new(right) blade

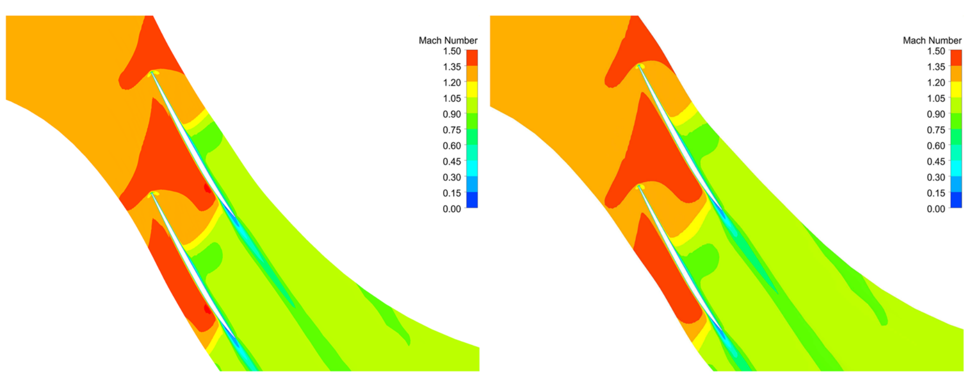

Fig. 17 The flow at 90% span of Rotor 67 between the original(left) and new(right) blade

Table 1 The comparison of aerodynamic performance before and after the modification

Name	Original	Redesigned
Pressure ratio	1.653	1.662
Efficiency	90.6%	91.1%
Mass flow	33.984	34.324

30% span is significantly reduced, while the flow field above 50% span is almost unchanged, indicating that the purpose of the modification near the hub of the blade is achieved.

In order to further quantitatively analyze the aerodynamic performance of the Rotor 67 before and after the modification, Table 1 shows the pressure ratio, efficiency at the near-peak-efficiency point.

From the above table, the result shows the modified design near the hub reduces the flow separation, thereby improving the overall aerodynamic performance of the blade and achieving the expected modification goal.

5 Conclusion

This paper demonstrates an improved inverse method on the basis of S1 stream surface solver of transonic axial compressors. In the improved method, a new inverse design boundary condition is developed based on the conservation of Riemann invariant and the theory of loading-camber method. On the one hand, the condition links the changes of the blade geometry with the flow parameters; on the other hand, the method strengthens the stability of the convergence procedure. Furthermore, a strict inverse design time step method is adopted to accelerate the calculation course and enhance the robustness. Afterward, typical cases are employed to verify the effectiveness of the reduced-order model and inverse design method. Finally, a partial modification on a transonic fan which achieves the desired goal is constructed by this paper. The novelty of the research work in this paper can be summarized as the following three points:

(1) Independently develops a flow solver based on the reduced-order model. The model fully considers the influence of the radius of the flow surface and the thickness of the flow sheet on the internal flow of the blade, and applies it to a typical axial compressor, which verifies the practicality and reliability of the flow solver.
(2) A new inverse method theory is proposed. This method combines the loading-camber method and pressure-profile method based on the conservation of Riemann invariant. Research results show that the method is more stable and effective.
(3) A fast modification method for the 3D blade geometry is developed. Compared with the two-dimensional method, the quasi-three-dimensional method fully considers the authenticity of the internal flow in the blade channel; compared with the full three-dimensional method, the quasi-three-dimensional method shows higher efficiency in calculation and more flexibility in the design process.

In conclusion, the improved inverse method based on the quasi-three-dimensional equations provides an efficient approach for partial modification of axial compressors.

Declarations

Conflict of interest The authors declared no potential competing financial interests with respect to the research, authorship, and/or publication of this article.

References

1. Kuzenov VV, Ryzhkov SV, Varaksin AY (2022) Calculation of heat transfer and drag coefficients for aircraft geometric models. Appl Sci 12(21):11011
2. Yang J, Wang R, Zhang M, Liu Y (2021) Parametric study of rotor tip squealer geometry on the aerodynamic performance of a high subsonic axial compressor stage. J Braz Soc Mech Sci Eng 43:1–13
3. Lighthill MJ (1945) A new method of two-dimensional aerodynamic design. Aero.res.council London R & M 2112
4. Stanitz JD (1952) Design of two-dimensional channels with prescribed velocity distributions along the channel walls. Technical Report Archive & Image Library (1115)
5. Hawthorne WR, Wang C, Tan CS, Mccune JE (1984) Theory of blade designfor large deflections: Part i—two-dimensional cascade. J Eng Gas Turbines Power 106(2):346–353
6. Tan CS, Hawthorne WR, McCune JE, Wang C (1984) Theory of blade designfor large deflections: Part ii—annular cascades. J Eng GasTurbines Power 106(2):354–365
7. Dulikravich G (1995) Shape inverse design and optimization for three-dimensional aerodynamics. In: Aerospace sciences meeting & exhibit
8. Dang T (1992) A fully three-dimensional inverse method for turbomachinery blading in transonic flows. In: Turbo Expo: Power for Land, Sea, and Air, vol 78934. American Society of Mechanical Engineers, pp 001–01070
9. Dang T (1995) Inverse method for turbomachine blades using shock-capturing techniques. In: 31st Joint Propulsion Conference and Exhibit, p 2465
10. Qiu X, Dang T (2000) 3d inverse method for turbomachine blading with splitter blades. In: Turbo Expo: Power for Land, Sea, and Air, vol 78545. American Society of Mechanical Engineers, pp 001–03090
11. Hield P (2008) Semi-inverse design applied to an eight stage transonic axial flow compressor. In: Asme Turbo Expo: Power for Land, Sea, & Air

12. Rooij MPCV, Dang TQ, Larosiliere LM (2008) Enhanced blade row matching capabilities via 3d multistage inverse design and pressure loading manager. In: Asme Turbo Expo: Power for Land, Sea, & Air
13. Rooij MPCV, Dang TQ, Larosiliere LM (2005) Improving aerodynamic matching of axial compressor blading using a 3d multistage inverse design method. In: ASME Turbo Expo 2005: Power for Land, Sea, and Air, vol 6 pt.B
14. Rooij MV, Medd A (2012) Reformulation of a three-dimensional inverse design method for application in a high-fidelity cfd environment. In: Asme Turbo Expo: 20 Turbine Technical Conference & Exposition
15. Zangeneh M, Goto A, Harada H (1997) On the design criteria for suppression of secondary flows in centrifugal and mixed flow impellers. J Turbomach 120(4):723–735
16. Tiow W, Zangeneh M (2000) A three-dimensional viscous transonic inverse design method. In: Turbo Expo: Power for Land, Sea, and Air, vol 78545. American Society of Mechanical Engineers, pp 001–03089
17. Zangeneh M, Goto A, Harada H (1999) On the role of three-dimensional inverse design methods in turbomachinery shape optimization. Proceedings of the Institution of Mechanical Engineers, Part C: Journal of Mechanical Engineering Science 213(1):27–42
18. Ramamurthy R, Ghaly W (2010) Dual point redesign of an axial compressor airfoil using a viscous inverse design method. In: Asme Turbo Expo: Power for Land, Sea, & Air
19. Jin-Guang Y, Zhen-De L, Fu-Yong S, Hu W (2015) A study of applications of 3d viscous inverse method based on transpiration boundary conditions for turbomachinery aerodynamic design. J Propulsion Technol 36(5):8
20. Jin-Guang Y, Zhen-De L, Fu-Yong S, Hu W (2015) Transpiration boundary condition based on inverse method for turbomachinery aerodynamic design: on the solution existence and uniqueness. J Propuls Technol 4:579–586
21. Zhao-wei L Research of full three dimensional viscous inverse design method for multi-stage axial compressor. PhD thesis, Northwestern Polytechnical University
22. Liu Y, Wang X, Yang J, Wu H (2017) An improved steady inverse method for turbomachinery aerodynamic design. Inverse Probl Sci Eng 25(5):633–651
23. Yang C, Wu H, Liang Y (2019) A novel three-dimensional inverse method for axial compressor blade surface design. Arab J Sci Eng 44(12):10169–10179
24. Jameson A, Schmidt W, Turkel E (1981) Numerical solution of the euler equations by finite volume methods using runge kutta time stepping schemes. In: AIAA, fluid and plasma dynamics conference, 14th, Palo Alto, CA, June 23-25, 1981. 15 p
25. Baldwin BS (1978) Thin-layer approximation and algebraic model for separated turbulent flows. pp 78-257
26. Blazek J (2015) Computational fluid dynamics: principles and applications, third edition. Elsevier, Amsterdam
27. Strazisar AJ, Wood JR, Hathaway M, Suder KL (1981) Laser anemometer measurements in a transonic axial-flow fan rotor. J Eng Gas Turb Power 103(2):430–437
28. Niehuis R, Bohne A, Hoynacki A (2003) Experimental investigation of unsteady flow phenomena in a three-stage axial compressor. Proc Instit Mech Eng Part A: J Power Energy 217(4):341–348